

ORIGIN OF TWO DISTINCT POPULATIONS IN DWARF SPHEROIDAL GALAXIES

DAISUKE KAWATA^{1,2}, NOBUO ARIMOTO³, RENYUE CEN⁴, AND BRAD K. GIBSON²

Submitted to ApJ

ABSTRACT

We study the chemical and kinematic properties of the first galaxies which formed at a high redshift, using high resolution cosmological numerical simulations, and compared them with the recent observational results for the Sculptor dwarf spheroidal galaxy by Tolstoy et al., who found two distinct stellar populations: the lower metallicity stars are more spatially extended and possess a higher velocity dispersion than the higher metallicity stars. Our calculations reproduce these observations as the result of a steep metallicity gradient, within a single populations, induced by dissipative collapse of the gas component. We also predict strong [N/O] enhancements in the lowest metallicity stars in dwarf spheroidals, due to the preferential retention of ejected gas from intermediate mass stars, compared to Type II supernovae.

Subject headings: galaxies: abundances — galaxies: kinematics and dynamics — galaxies: formation — galaxies: stellar content — galaxies: individual (Sculptor)

1. INTRODUCTION

Dwarf galaxies in the Local Group are one of the prime observational targets for galactic astronomy, because their relatively short distances enable us to observe the properties of individual stars, which provide great details of their formation history (Baade 1944). Dwarf Spheroidals (dSphs) are one of the most populous dwarf galaxy type seen in the Local Group, and are defined as galaxies with $M_B > -14$ mag, low surface brightness ($\mu_V > 22$ mag arcsec $^{-2}$), no well-defined nucleus (although in some dSphs, like Fornax and Sagittarius, a globular cluster seems to correspond to nucleus), and very little gas (Gallagher & Wyse 1994; Grebel 1997; Mateo 1998). They do not have any ongoing star formation. Some of them do not have any intermediate-age stars at all. On the other hand, our current favorite Λ -dominated cold dark matter (Λ CDM) cosmology suggests that small objects form first, and larger systems are built up by the assembly of smaller systems (e.g. White & Rees 1978). Therefore, it is considered that dSphs might be the first generation of galaxies and survived from cannibalization by larger systems. Hence, dSphs might contain a record of the epoch of the end of the dark age. Recently, using a cosmological numerical simulation, Ricotti & Gnedin (2002) demonstrated that the small galaxies formed at high redshifts can explain the global properties, such as the luminosity, velocity dispersion, and iron abundance, of the dwarf galaxies observed in the Local Group. Their study encourages us to make a further investigation of the connection between the first galaxies and the dSphs.

With the wide field multi-object spectrograph, *FLAMES* on the *Very Large Telescope*, Tolstoy et al. (2004) (T04) have measured the metallicity and line-of-sight velocity for 300 member stars, distributed over a

large radial range (~ 20 times its core radius), in the Sculptor (Scl) dSph galaxy. They found that the stars in the Scl dSph show two distinct populations. One of them is more metal rich ($[\text{Fe}/\text{H}] \sim -1.4$) with a centrally concentrated distribution. The other one is metal-poor ($[\text{Fe}/\text{H}] \sim -2$) and more spatially extended. In addition, the higher metallicity stars show lower velocity dispersion than the lower metallicity stars. This is unprecedented information to unveil the formation history of the Scl dSph.

To disentangle the formation process of the dSph from such observational data, we construct a theoretical model which can be compared with the observations. The aim of this paper is to show our first attempt to make a self-consistent numerical simulation model which can be compared with the observational data of the Scl dSph directly and quantitatively. We pay particular attention to the radial trend of iron abundance and velocity dispersion, to compare with the unprecedently detailed observation presented in T04, which are not discussed in Ricotti & Gnedin (2002). The next section describes our numerical method. Section 3 presents our simulation results and comparison with the observational data in T04. Discussion and conclusion are seen in Section 4.

2. NUMERICAL METHODS

In this study we focus on the properties of a dwarf galaxy which formed at a high redshift in our high resolution cosmological simulation. The simulation was carried out using the galactic chemodynamics code, *GCD+* (Kawata & Gibson 2003a). *GCD+* is a three-dimensional tree N -body/smoothed particle hydrodynamics (SPH) code which incorporates self-gravity, hydrodynamics, radiative cooling, star formation, supernovae (SNe) feedback, and metal enrichment. *GCD+* takes account of the chemical enrichment by both Type II (SNe II) and Type Ia (SNe Ia) SNe, mass-loss from intermediate mass stars, and follows the chemical enrichment history of both the stellar and gas components of the system. To study the formation process of small systems, we update the code to implement non-equilibrium chemical reactions of hydrogen and helium species (H , H^+ , He , He^+ ,

¹ The Observatories of the Carnegie Institution of Washington, 813 Santa Barbara Street, Pasadena, CA 91101

² Swinburne University of Technology, Hawthorn VIC 3122, Australia

³ National Astronomical Observatory, 2-21-1 Osawa, Mitaka, Tokyo 181-8588

⁴ Department of Astrophysical Sciences, Princeton University, Peyton Hall, Ivy Lane, Princeton, NJ 08544

He^{++} , H_2 , H_2^+ , H^-) and their cooling processes. The details of the updated code is described in Appendix A.

We adopt a ΛCDM cosmology of $\Omega_0 h^2 = 0.135$, $\Lambda_0 = 1 - \Omega_0$, $\Omega_b h^2 = 0.0224$ and $h = 0.71$, (Spergel et al. 2003), and use a multi-resolution technique (Kawata & Gibson 2003b) to achieve high-resolution in the regions of interest, while outer regions exerting the tidal forces are handled with lower resolution. The initial conditions for the simulations are constructed using the public software **GRAFIC2** (Bertschinger 2001). Gas dynamics and star formation are included only within the relevant high-resolution region (~ 80 kpc in comoving scale); the surrounding low-resolution region (~ 530 kpc diameter sphere) contributes to the high-resolution region only through gravity. Consequently, the initial condition consists of total 287,491 dark matter particles and 233,280 gas particles. The mass and softening length of individual gas (dark matter) particles in the high-resolution region are 129 (650) M_\odot and 30 (51) pc, respectively.

To reduce the computational cost, we applied the significantly small simulation volume. Hence, our simulation misses the density perturbation induced by larger scale modes. Figure 1 demonstrates that the mass variance, $\sigma(M)$, becomes slightly smaller at the mass scale which we are interested in ($\sim 10^8 M_\odot$), if the power spectrum for wavelengths longer than our simulation volume are ignored. In addition, the first galaxies are expected to form at high density peaks, i.e. biased regions (Mo & White 1996). Therefore, we adopt a higher value of $\sigma_8 = 1.8$, instead of a value suggested by recent observations ($\sigma_8 = 0.9$). Figure 1 also shows the mass variance for the applied power spectrum. The adopted high σ_8 value enables us to form a relevant dSph-like small galaxy in the particular realization with the relatively small simulation volume, in addition to partly compensate for the missing waves larger than our simulation box.

In the high-resolution region, we found a small stellar system at $z = 5.9$ (Figure 2). The virial radius and mass of this system are respectively 1.9 kpc and $5.1 \times 10^7 M_\odot$ at $z = 5.9$. Here, we follow the fitting formula in Appendix of Kitayama & Suto (1996) to define the virial mass and radius, taking into account the cosmology and redshift. We assume that at this redshift star formation in this system has been quenched by mechanisms, such as re-ionization (e.g. Efstathiou 1992; Chiba & Nath 1994; Thoul & Weinberg 1996; Bullock et al. 2000; Benson et al. 2002; Susa & Umemura 2004b) and/or galactic wind (e.g. Dekel & Silk 1986; Arimoto & Yoshii 1987), and the system evolves passively afterwards. Thus, we assume that the chemical and kinematic properties at $z = 5.9$ would not change till $z = 0$, and we analyze the properties expected at $z = 0$ from the output of the simulation at $z = 5.9$. This is, of course, consistent with our assumption that the observed dSph is a galaxy that formed early and retained its own identity until $z=0$. We will check this ansatz by examining its detailed properties.

The middle panel of Figure 2 shows the rest-frame V -band luminosity distribution of this galaxy at $z = 5.9$. The luminosity distribution is calculated by our population synthesis code, taking account of the metallicity and age of the star particles at $z = 5.9$. We use the single stellar population spectrum data in Kodama & Arimoto (1997). The data do not include any emission lines. For

simplicity, we do not take into account any absorption by the inter-stellar (ISM) and inter-galactic medium (IGM). To make sure that the system is dynamically stable and the distribution of stellar population and kinematics does not change till $z = 0$ dramatically, we run a pure N-body simulation using the particles within a radius of ~ 1.7 times the virial radius at $z = 5.9$, as an initial condition. We run this N-body simulation (relaxing run) for about five Gyr (corresponding to the time from $z = 5.9$ to $z = 1$). The right panel of Figure 2 shows the rest-frame V -band luminosity distribution analyzed from the final output of this relaxing run extrapolated at $z = 0$, based on the stellar age at $z = 0$. Figure 3 shows the V -band surface brightness profiles for the system before (open circles) and after (solid circles) the relaxing run. The profile after the relaxing run is similar to the profile before. We also confirmed that all the properties presented in this paper are not changed after the relaxing run. Therefore, the properties at $z = 5.9$ are expected to be unchanged till $z = 0$. We present only the results from the data after the relaxing run in the next section.

The solid line in Figure 3 represents a King profile with the core radius, r_c , and tidal radius, r_t , same as the observed values in the Scl dSph, i.e. $r_c = 0.12$ kpc and $r_t = 1.6$ kpc. We assume the distance of the Scl dSph is 72 kpc (Kunkel & Demers 1977, T04). The central surface brightness is normalized to roughly match with the simulated surface brightness profile. In the inner region, the simulated system has a similar profile to the observed profile of the Scl dSph, which means that the simulated galaxy has a similar core radius. In the outer region, the simulated galaxy has higher surface brightness compared to the King profile. Therefore, the tidal radius of the simulated galaxy is inconsistent with the observed one. However, our simulated galaxy is an isolated system, while the Scl dSph is a satellite galaxy of the Milky Way. We expect that if the simulated galaxy falls into a bigger host galaxy, the stars in the outer region are tidally stripped, and thus the tidal radius would depend on their environment, which could make the tidal radius of the simulated galaxy smaller and similar to the observed one. Here, we assume that such stripping does not change the properties of the inner region, and compare the properties of this isolated system with those of the Scl dSph.

The basic properties of the simulated galaxy are summarized in Table 1. In the next section, we compare our model results with the observational data of the Scl dSph in T04.

3. RESULTS

Figure 4 shows the formation history of this galaxy. Although some minor mergers are involved, the system is forming in a monolithic way. The lower panel of Figure 5 shows the virial mass evolution of the galaxy and building blocks which merge into the galaxies. The panel demonstrates that the main system experiences only two minor mergers (mass ratio smaller than 0.4). The upper panel of Figure 5 shows the history of the star formation rate (SFR). In this galaxy, star formation starts at $z = 25.5$, and the SFR has a peak around $z = 15$. The $z = 17.2$ panel in Figure 4 shows that the gas is blown out and the heavy elements are distributed to the IGM. Table 2 presents the heavy element mass budget for the stars

TABLE 1
BASIC MODEL RESULTS

M_{vir} (M_{\odot})	r_{vir} (kpc)	$M_{\text{gas}}(< r_{\text{vir}})$ (M_{\odot})	$M_{\text{DM}}(< r_{\text{vir}})$ (M_{\odot})	$M_{\text{star}}(< r_{\text{vir}})$ (M_{\odot})	M_V (mag)	$T_{\text{vir}}^{\text{a}}$ (K)
5.1×10^7	1.9	3.5×10^5	5.0×10^7	1.9×10^5	-7.23	2.8×10^3

^aVirial temperature calculated by $GM_{\text{vir}}\mu m_p/3k_B r_{\text{vir}}$ (Kitayama & Suto 1996).

TABLE 2
HEAVY ELEMENT MASS BUDGET FOR THE SYSTEM WITHIN
 r_{vir} .

$z = 12.1$			$z = 5.9$			
	$M_{Z,\text{ej}}^{\text{a}}$ (M_{\odot})	$M_{Z,\text{s}}^{\text{b}}$ (M_{\odot})		$M_{Z,\text{ej}}^{\text{a}}$ (M_{\odot})	$M_{Z,\text{s}}^{\text{b}}$ (M_{\odot})	
N	17.0	2.5	0.85	160.0	32.0	0.80
O	170.0	14.0	0.92	1900.0	330.0	0.82
Fe	17.0	0.63	0.96	150.0	14.0	0.91

^aTotal ejected mass.

^bMass in stellar component.

^cEscape fraction.

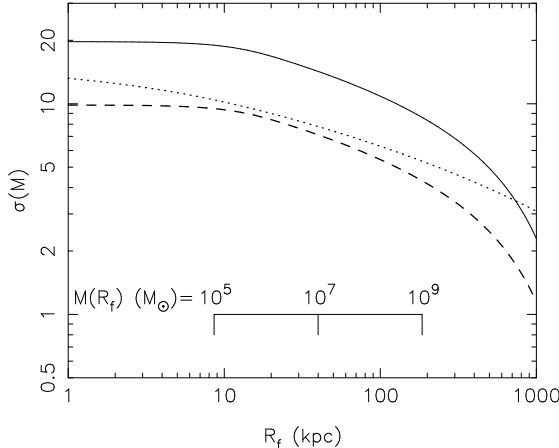


FIG. 1.— The mass variance for the CDM power spectrum as a function of filter radius, R_f . The mass corresponding to the filter radius, $M(R_f)$, is also shown in the panel. The dotted line shows the mass variance with $\sigma_8 = 0.9$. The dashed line indicates the same as dotted line, but the power spectrum for the wave-length longer than our simulation volume (~ 530 kpc) and shorter than Nyquist wave-length (~ 22 kpc) are ignored. The solid line demonstrates the same as the dashed line, but with $\sigma_8 = 1.8$, i.e. our applied power spectrum.

which are within the virial radius at $z = 5.9$. The total ejected mass, $M_{Z,\text{ej}}$, means the mass of each heavy element ejected from stars within r_{vir} till that redshift. The mass in stellar component, $M_{Z,\text{s}}$, is defined as the mass of each heavy element still within the stellar component within the virial radius. We define the escape fraction as $f_{\text{esc}} = 1.0 - M_{Z,\text{s}}/M_{Z,\text{ej}}$. Here, we consider that the heavy elements in the gas component are also blown out after some mechanism stops star formation at $z = 5.9$. Table 2 indicates that more than 80 % of the heavy elements produced in stars have escaped from the system till $z = 5.9$. Our assumed SNe feedback (7.5×10^{50} erg per supernova which is chosen to reproduce the low metallicity of the Scl dSph) has a strong effect on the gas dynam-

ics, and continuously blows out the gas from the system. However, the continuous gas accretion leads to further star formation, albeit at a somewhat lower rate. Figure 5 displays that star formation continuously occurs even around this blow-out phase. Nevertheless, star formation of this small system is strongly suppressed by SNe feedback, which helps to keep the stellar metallicity low, as seen in the age-metallicity relation shown in the right panel of Figure 6.

As described in Section 1, T04 found that the stars in the inner region have higher metallicity than those in the outer region. They split the two regions at the radius of about 0.25 kpc, and demonstrated that the metallicity distribution function (MDF) of stars in the inner (outer) region has a peak around $[\text{Fe}/\text{H}] = -1.4$ (-2.0). To compare with their result, Figure 7 shows the MDF for stars in the inner ($R < 0.25$ kpc⁵) and outer ($R > 0.25$ kpc) regions for our simulated galaxy. The MDF for the inner (outer) region of the simulated galaxy has a peak at $[\text{Fe}/\text{H}] \sim -1.4$ ($[\text{Fe}/\text{H}] \sim -1.9$), which is in good agreement with the observed MDFs in T04. Therefore, the simulated galaxy also show two distinct stellar populations.

We found that this is just due to the metallicity gradient in the system. Figure 6 shows the peak of the metallicity distribution at different radii gradually decreases, as the radius increases, i.e. there is a metallicity gradient in the simulated system. Since the metallicity gradient is steep enough in the system, the MDF for the inner region moves toward higher $[\text{Fe}/\text{H}]$, compared to the MDF for the outer region. This demonstrates that the steep metallicity gradient can make the two different chemical properties in the inner and outer regions.

Next, we analyze the kinematic properties. Figure 8 presents the velocity dispersion at different radii for the low ($[\text{Fe}/\text{H}] < -1.7$) and high ($[\text{Fe}/\text{H}] > -1.7$) metallicity stars. This velocity dispersion is obtained by taking the line-of-sight velocity dispersion of stars within annuli at different radii. To improve the statistics, we analyzed the line of sight velocity at 36 different projections, and obtained the velocity dispersion. Figure 8 also shows the observed velocity dispersion of the low ($[\text{Fe}/\text{H}] < -1.7$) and high ($[\text{Fe}/\text{H}] > -1.7$) metallicity stars in T04. Within the radius of about 0.6 kpc, the observational data show that the velocity dispersion of the high metallicity stars is lower than that of the low metallicity stars⁶. In other words, the two different metallicity components also have distinctive dynamical properties. Our simulation results also show the same trend,

⁵ Throughout this paper, R represents radius at an arbitrary projection, and we ignore the stars $R > 2.5$ kpc.

⁶ Note that T04 mentioned that in the region outside of the radius of 0.6 kpc, the number of the high metallicity stars are too small.

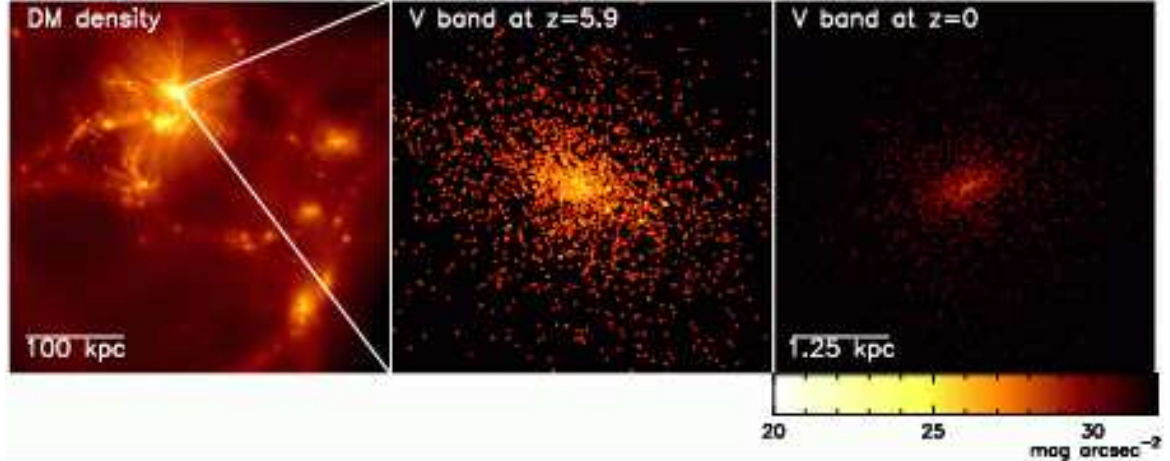


FIG. 2.— Dark matter density distribution at $z = 5.9$ (left), V -band (rest-frame) luminosity distribution at $z = 5.9$, and expected V -band luminosity distribution at $z = 0$ after the passive evolution.

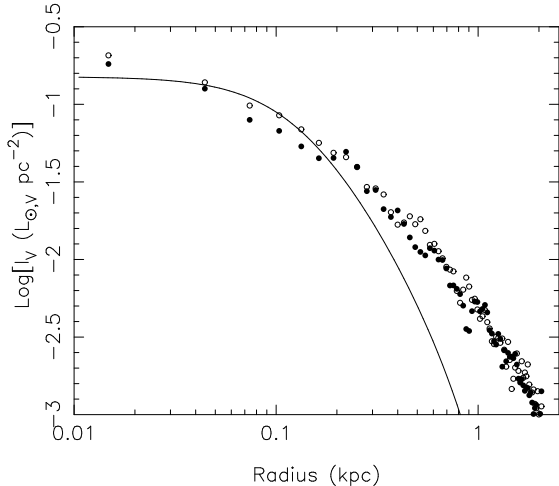


FIG. 3.— The V -band surface brightness profile from the simulation data before (open circles) and after (solid circles) the relaxing run (see text for details). The solid line presents a King profile with the core radius, $r_c = 0.12$ kpc, and tidal radius, $r_t = 1.6$ kpc.

although the difference is small.

Our simulation demonstrates that a system formed at a high redshift can reproduce the two stellar populations whose chemical and dynamical properties are distinctive. However, the simulated galaxy shows some inconsistent results with the observed properties of the Scl dSph. First, compared with Figure 3 of T04, the MDFs for both inner and outer regions of the simulated galaxy have a too long tail at lower $[\text{Fe}/\text{H}]$. In the observational data, there are no stars at $[\text{Fe}/\text{H}] < -2.8$, although T04 selected their samples from the limited region of the color-magnitude diagram, which might tend to exclude too low and too high metallicity stars. On the other hand, the simulated galaxy has a significant fraction of stars with such low metallicity. Next, Figure 8 also shows that the velocity dispersion of our simulated galaxy is too small compared with the observed values. In addition, Table 1 presents that the V -band magnitude of the simulated galaxy ($M_V = -7.23$), which is also small, compared with the luminosity of the Scl dSph ($M_V = -10.7$). These are problems of our current model, which are required to be solved in a future study, and we will discuss possible solutions in the next section.

Finally, we have also analyzed abundance ratios. Tolstoy (2005) presents that the stars in the Scl dSph show different distributions in the $[\alpha/\text{Fe}]$ versus $[\text{Fe}/\text{H}]$ plane, compared with the stars in the solar neighborhood (see also Shetrone et al. 2003; Geisler et al. 2005). In the Scl dSph, $[\alpha/\text{Fe}]$ of the member stars with $[\text{Fe}/\text{H}] < -2$ are higher than solar abundance ratios, and $[\alpha/\text{Fe}]$ approach the solar value as $[\text{Fe}/\text{H}]$ increases at $[\text{Fe}/\text{H}] > -2$. On the other hand, in the solar neighborhood $[\alpha/\text{Fe}]$ are constantly higher than the solar value for the stars with $[\text{Fe}/\text{H}] < -1$, and starts decreasing at $[\text{Fe}/\text{H}] = -1$. This difference can be explained by the contribution from SNe Ia, which decreases $[\alpha/\text{Fe}]$, and a lower star formation rate in the dSph, which keeps $[\text{Fe}/\text{H}]$ low till the chemical enrichment by SNe Ia becomes important (e.g. Ikuta & Arimoto 2002). However, Figure 9 demonstrates that in the simulated galaxy, the mean $[\text{O}/\text{Fe}]$ is almost constant (oxygen is one of typical α -elements). One reason why there is no enrichment from SNe Ia is because we implemented a SNe Ia model proposed by Kobayashi et al. (2000) who suggested that SNe Ia are inhibited in the stars with $[\text{Fe}/\text{H}] < -1$. Even if we relax their $[\text{Fe}/\text{H}]$ limit for SNe Ia, it is difficult to explain the observational trend. Kobayashi et al. (2000) consider that the mass ranges of companion stars for the SNe Ia progenitor binaries are restricted to between 0.9 and $1.5 M_\odot$ (they call RS+WD system) and between 1.8 and $2.6 M_\odot$ (MS+WD system). The expected lifetime of $2.6 M_\odot$ stars with $\text{Log}(Z/Z_\odot) = -2.3$ are about 0.5 Gyr, according to the lifetime used in Kodama & Arimoto (1997). On the other hand, Figures 5 and 6 indicate that the stars with $[\text{Fe}/\text{H}] > -2$ start forming even 0.1 Gyr after the first star formation. However, the progenitors of SNe Ia are still unknown. For example, another SNe Ia progenitor model suggested by Greggio & Renzini (1983) consider that the mass range of the binaries is between 8 and $3 M_\odot$. Since the lifetime of such stars is 0.03 – 0.3 Gyr, if we applied their model, the observational trend of $[\text{O}/\text{Fe}]$ and $[\text{Fe}/\text{H}]$ could be explained. Another solution to explain the decrease in $[\alpha/\text{Fe}]$ is increasing the contribution of SNe II from stars with the mass between 10 and $15 M_\odot$ whose yields provide $[\alpha/\text{Fe}] < 0$ (e.g. Woosley & Weaver 1995; Gibson 1997). However, the observed trend of the decreasing $[\alpha/\text{Fe}]$ requires a fine-tuned variation of the shape of the IMF, depending on metallicity,

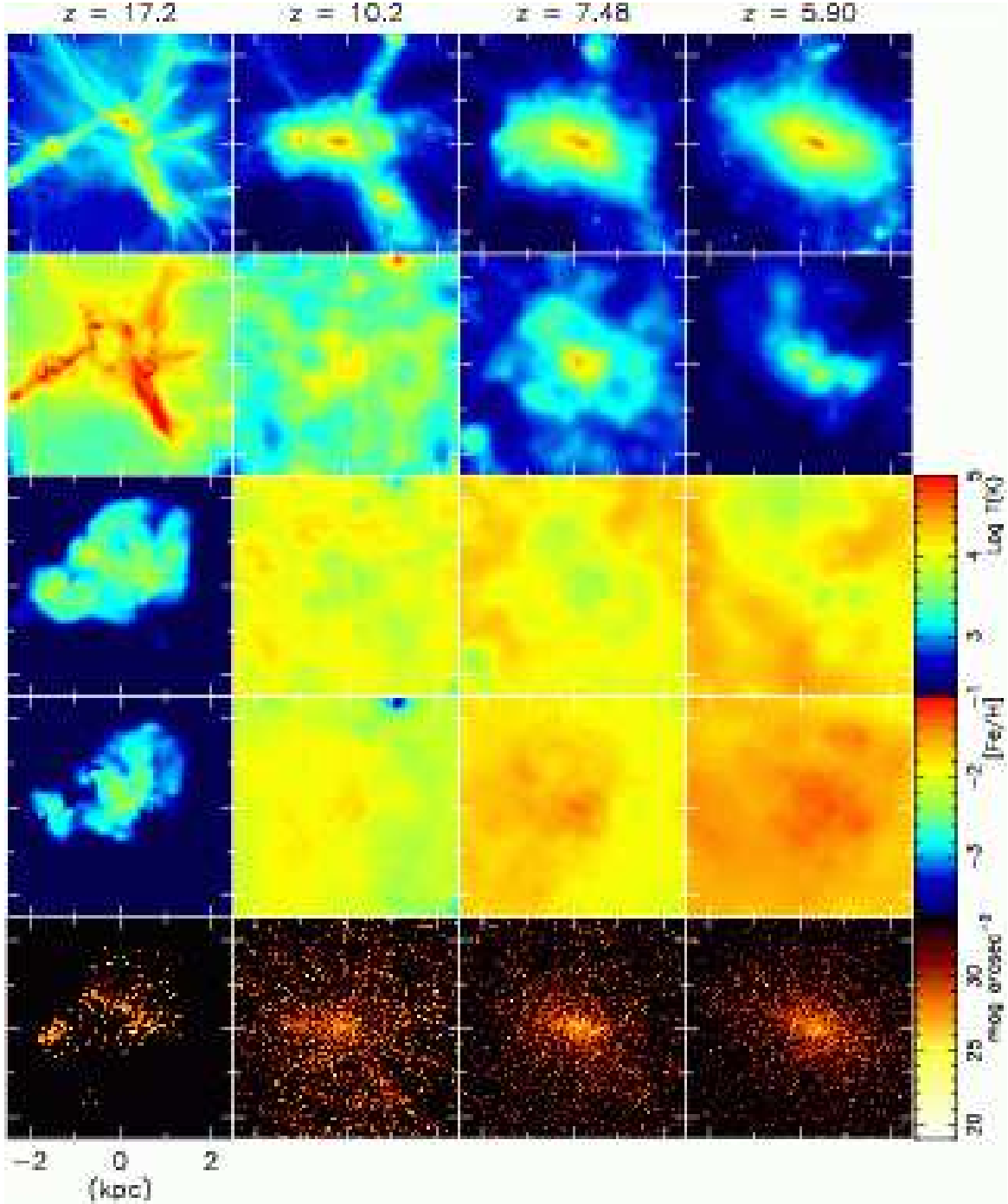


FIG. 4.— Evolution of the distributions of dark matter density (top), the gas density (2nd), the gas temperature (3rd), the iron abundance of gas (4th), and K -band (observed-frame) luminosity (bottom).

which seems unlikely.

Figure 9 also shows that the simulated $[\mathrm{O}/\mathrm{Fe}]$ has too large a scatter, compared with the observational data. The particles with a low $[\mathrm{Fe}/\mathrm{H}]$ are likely enriched only a few times, and then their abundance pattern reflects that of the yields from the stars within a small mass range. As a result, the scatter of $[\alpha/\mathrm{Fe}]$ for the star particles becomes as big as $[\alpha/\mathrm{Fe}]$ variation of the yields of SNe II progenitors with different masses (Woosley & Weaver 1995). This indicates a serious problem of the current chemical evolution model in the particle based numerical simulation. The problem is also known in explaining

the small dispersion of $[\alpha/\mathrm{Fe}]$ for metal-poor halo stars ($[\mathrm{Fe}/\mathrm{H}] = -3 \sim -2$) in the Milky Way, which provides a strong constraint to the chemical evolution history of the Galaxy (e.g. Arnalte et al. 2005). So far numerical simulations of disk galaxy formation show clearly larger scatter than what is observed (see also Raiteri et al. 1996). This suggests that we have to consider some metal mixing model between particles. Nevertheless, the mean values of metallicity from the current simulation models may be relatively robust.

We also analyzed the abundance ratio of $[\mathrm{N}/\mathrm{O}]$ against $[\mathrm{O}/\mathrm{H}]$, and found an interesting feature. Figure 10

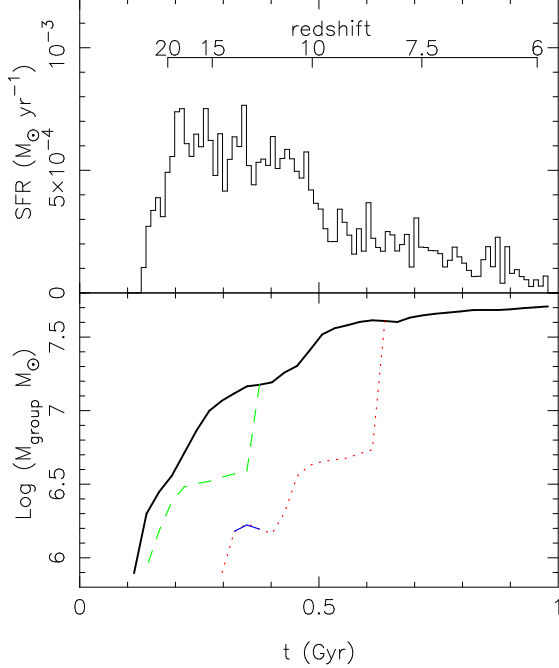


FIG. 5.— Time variation of the star-formation rate and the evolution of the virial mass of the progenitor halos. In the bottom panel, different styles of the lines (black thick-solid, red dotted, green dashed and blue thin-solid) indicate different halos. The connection between lines displays that two halos merge together. For example, the halo shown by red dotted line merges into the large halo described by black thick-solid line at $t \sim 0.64$ Gyr.

demonstrates that there is a visible trend that $[\text{N}/\text{O}]$ decrease from $[\text{N}/\text{O}] = 2$ to ~ 0 as $[\text{O}/\text{H}]$ increase from $[\text{O}/\text{H}] = -4$ to -1.5 . The middle panel of the figure also shows that high $[\text{N}/\text{O}]$ are seen in the stars formed around $t = 0.3$ Gyr, and the stars born at later epochs have lower $[\text{N}/\text{O}]$. This high $[\text{N}/\text{O}]$ comes from the stars with the mass between 4 and $8 M_{\odot}$ whose lifetime is around 0.1 Gyr (right panel of Figure 10). To make the contribution from such intermediate mass stars important, it is required to suppress the contribution from the higher mass stars whose $[\text{N}/\text{O}]$ are lower and whose lifetime is shorter. As seen in Figure 4, the enriched gas is blown out at a high redshift around $z = 17$, due to the strong feedback by SNe II and relatively shallow potential of the system at such a high redshift. As a result, the chemical enrichment by the massive stars, i.e. SNe II, becomes less important, and enrichment from the intermediate mass stars becomes relatively more important. As the system gets bigger and their gravitational potential can bound the gas enriched by SNe II, $[\text{N}/\text{O}]$ starts decreasing. This is also demonstrated in Table 2 which shows the metal budget at $z = 12.1$ and $z = 5.9$ (see above for details). At $z = 12.1$, the escape fraction of oxygen is significantly higher than nitrogen, and their values get closer at $z = 5.9$. Oxygen is mainly produced in SNe II, although they are still created in the intermediate mass stars (van den Hoek & Groenewegen 1997). On the other hand, nitrogen mainly comes from the intermediate mass stars. Thus, Table 2 indicates that the gas enriched by SNe II is preferentially blown out at high redshift. Therefore, testing this trend of $[\text{N}/\text{O}]$ in dSphs would be interesting. To our knowledge, the nitrogen abundance has not been observed in the dSphs. On the other hand, the intermediate mass

stars are also expected to be progenitors of s-process elements. Recent observational studies (e.g. Smecker-Hane & McWilliam 2002; Tolstoy et al. 2003; Sadakane et al. 2004; McWilliam & Smecker-Hane 2005b,a) suggest that the s-process elements are enhanced in the dSphs. This might be explained by the process that the SNe II enriched gas is preferentially blown out from the system, and the enrichment by the intermediate mass stars is more important in the dSph. Interestingly, Smecker-Hane & McWilliam (2002); McWilliam & Smecker-Hane (2005a) show that the s-process elements are more enhanced in higher metallicity stars in the Sagittarius dSph. In addition, Sadakane et al. (2004) found a very metal poor star ($[\text{Fe}/\text{H}] = -2.7$) which has anomalously low abundance of the s-process elements in the Ursa Minor dSph. This may indicate a delay of s-process elements enrichment, because s-process elements come from relatively low mass ($1.5 \sim 3 M_{\odot}$), i.e. long lifetime, stars.

4. DISCUSSION AND CONCLUSIONS

We have analyzed chemical and kinematic properties of a small system which formed at a high redshift in the ΛCDM cosmological simulation. Our simulated galaxy shows that the higher metallicity ($[\text{Fe}/\text{H}] > -1.7$) stars have more centrally concentrated distribution and lower velocity dispersion, compared with the lower metallicity stars ($[\text{Fe}/\text{H}] < -1.7$). This trend is consistent with the observed trend in the Scl dSph reported in T04. Thus, we conclude that a survivor of a small system which formed at a high redshift can explain the observed stellar chemical and kinematic properties.

T04 claimed that this observed trend indicates that there are two distinct populations in the Scl dSph. They argue three possible mechanisms to explain the two populations. 1) Two episodes of star formation: The subsequent SNe feedback from the initial star formation blows out the gas and stops star formation temporally. After SNe feedback gets weaker, more metal-rich gas comes back and forms new generation of stars (Carraro et al. 2001; Mori et al. 2002). 2) External influences, such as minor mergers or accretion of additional gas at later epoch. 3) Selected heating by the UV background radiation: The radiation evaporates the outer layers of the gas preferentially, and star formation lasts longer in the inner region (Susa & Umemura 2004a). Figure 5 shows that our simulated galaxy does not have two episodes of star formation. In this study, we assume that there is no later minor merger or gas accretion after star formation is stopped at the high redshift, and star formation is abruptly terminated without any time delay depending on the radius. Thus, the formation history of our simulated galaxy does not correspond to any above scenario.

Figures 4 and 5 show that the simulated galaxy forms rather monolithically. It is known that the monolithic collapse of the dissipative gas component leads to the higher metallicity for the gas in the inner region, because the gas which dissipatively accretes into the inner region are enriched by the stars in the outer region as well as the stars in the inner region where the stellar density is higher. As Figure 5 shows, the substantial duration of the starburst at $z = 13 \sim 20$ allows for significant self-enrichment in the inner region of the galaxy, resulting in a higher metallicity stellar population there. The outer regions are progressively less vigorous in the

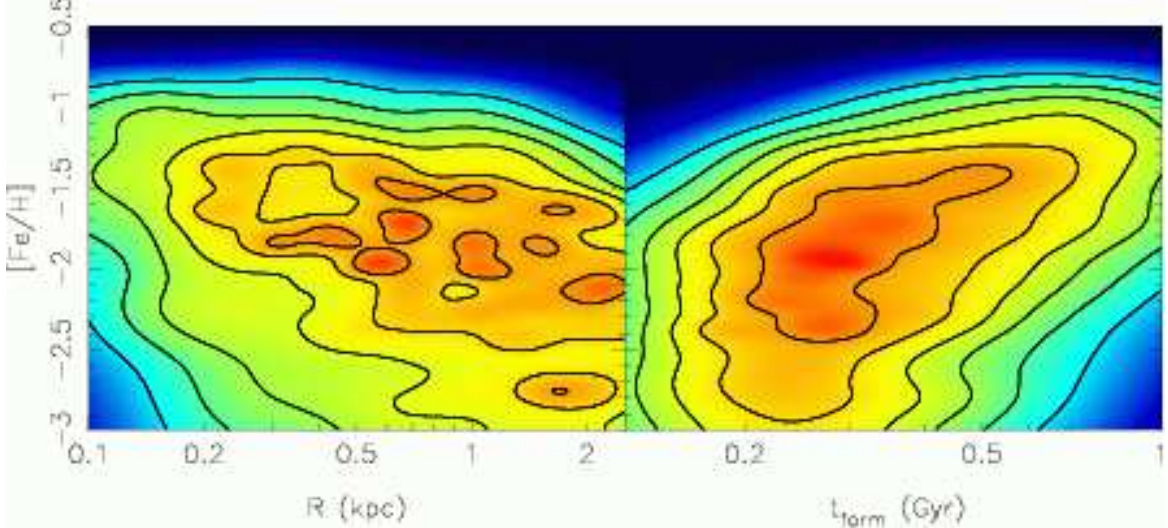


FIG. 6.— Smoothed stellar mass distribution in the $[\text{Fe}/\text{H}]$ vs. radius plane (left) and in the $[\text{Fe}/\text{H}]$ vs. formation time, t_{form} , plane, i.e. the age-metallicity relation (right).

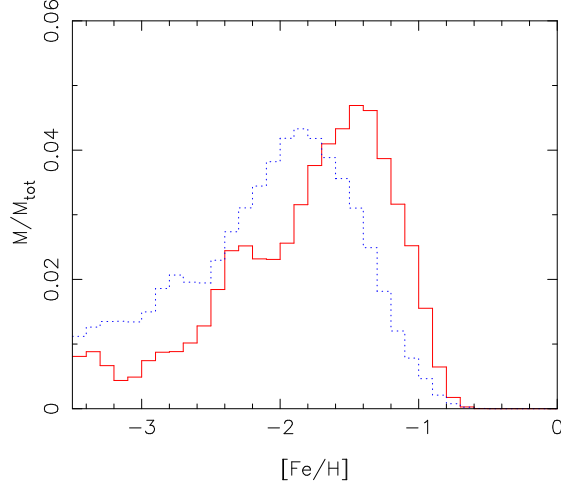


FIG. 7.— Metallicity distribution function of stars in the inner ($R < 0.25$ kpc: red solid histogram) and outer ($R > 0.25$ kpc: blue dotted histogram) region.

star formation activities due to supernova explosion feedback effect, which significantly reduces gas content of the galaxy as well as subsequent merger subunits. The latter point is clearly visible in Figure 5; for example, the merger event at $z \sim 8$ is not associated with any increased star formation activity, indicating lack of gas. This mechanism makes the mean metallicity of the stars in the inner region higher. This is the same mechanism as what is suggested to explain the metallicity gradient for larger spheroidals, i.e. normal elliptical galaxies (Larson 1974; Carlberg 1984; Kawata & Gibson 2003a; Kobayashi 2004). In fact, Figure 6 shows a metallicity gradient in the simulated system. Hence, our simulation demonstrates that for a small system, which stopped star formation at a high redshift, it is possible to have a metallicity gradient, which can explain the *apparent* two distinct populations observed in the dSph Scl stars. Note that the metallicity gradient has to be steep, to make such difference in the inner and outer region. Thus, if the steepness of the metallicity gradient is responsible for the apparent two populations in the dSph, and the metallicity gradients are different between dSphs like seen in elliptical

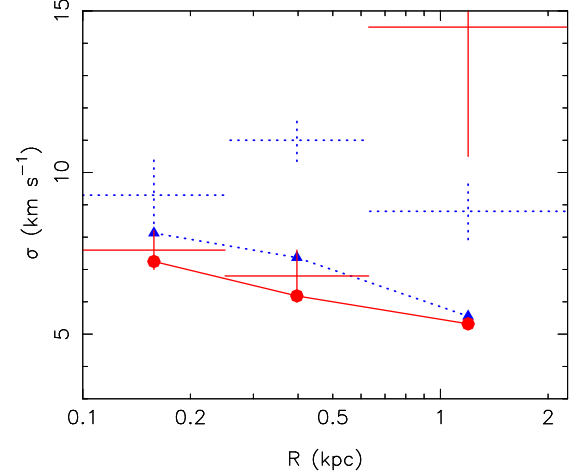


FIG. 8.— Velocity dispersion profile of high ($[\text{Fe}/\text{H}] > -1.7$: red circles connected with solid line) and low ($[\text{Fe}/\text{H}] < -1.7$: blue triangles connected with dotted line) metallicity stars. The observational data in T04 are also shown as the red solid (for $[\text{Fe}/\text{H}] > -1.7$) and blue dotted (for $[\text{Fe}/\text{H}] < -1.7$) crosses, where the horizontal-bar corresponds to the radial range, and the vertical-bar corresponds to their dispersion.

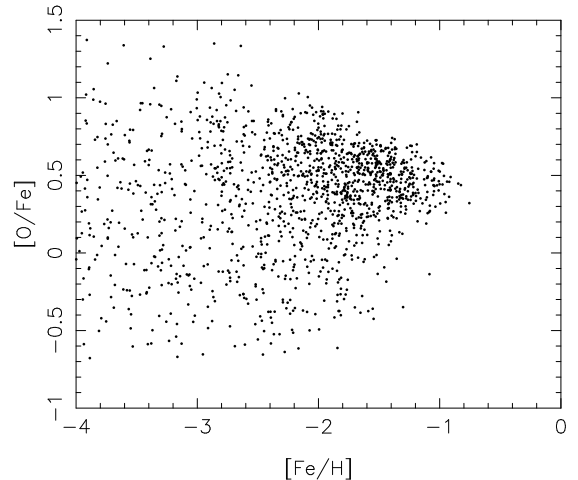


FIG. 9.— $[\text{O}/\text{Fe}]$ as a function of $[\text{Fe}/\text{H}]$ for star particles within $R = 2.5$ kpc.

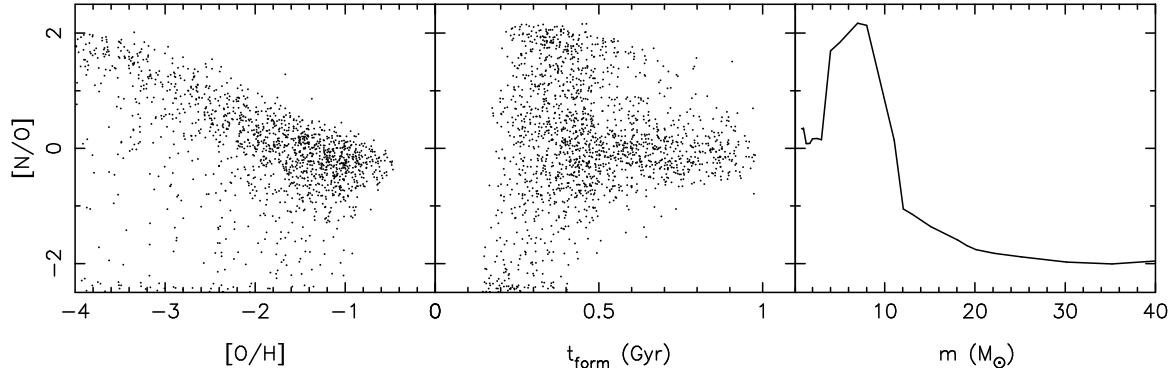


FIG. 10.— *Left:* $[\text{N}/\text{O}]$ as a function of $[\text{O}/\text{H}]$ for star particles within $R = 2.5$ kpc. *Middle:* $[\text{N}/\text{O}]$ as a function of their formation epoch. *Right:* $[\text{N}/\text{O}]$ yields as a function of the mass of the progenitor stars with metallicity of $Z/Z_{\odot} = 0.01$ (Woosley & Weaver 1995; van den Hoek & Groenewegen 1997).

galaxies (e.g. Kobayashi & Arimoto 1999), there may be a dSph which does not show such two populations due to less steep metallicity gradient. Thus, it would be important to obtain more sample of both simulated and observed dSphs.

Unfortunately, some properties of our simulated galaxy are inconsistent with those observed in the Scl dSph. Figure 7 shows that in both inner and outer region there are significant amount of stars which have extremely low metallicity. This is the same problem as so-called “G-dwarf problem” known from the difficulty for a simple chemical evolution model to explain the MDF of the G-dwarfs in the solar neighborhood (e.g. van den Bergh 1962; Tinsley 1975) and to reproduce the spectrum features in the central region of bright elliptical galaxies (e.g. Arimoto & Yoshii 1987; Bressan et al. 1994; Greggio 1997). The solution suggested for the solar neighborhood G-dwarf problem include a) gas infall, b) prompt initial enrichment (PIE), and c) metal-enhanced star formation (MESF). The infall model has been so far very successful in solving the local G-dwarf problem, as it is likely that the disk of the Milky Way has been formed by continuous accretion of gas from the reservoirs, such as the Galactic halo gas and the IGM. However, our simulation already takes into account cosmological gas infall. Hence, the infall model unlikely works for interpretation of the MDF of the dSph. The MESF model is unlikely either, as it is also fully taken into account in our simulations by introducing radiative cooling rate depending on the metallicity of the gas particles. This leaves the PIE scenario as the most attractive possibility for solving the G-dwarf problem of the dSph galaxies. The possible mechanism would be that at high redshift ($z \sim 20$) Population III stars formed at the center of the building block, and the supernova explosions blew up the gas in the building blocks, which helps to enrich the IGM. Then, the enriched gas re-infalled to the system which got bigger after multiple mergers of building blocks, and Population II stars were produced from the enriched gas. If the lifetime of the lowest-mass Population III stars is shorter than the Hubble time, the Population III stars do not exist at the current dSph. Although the first building blocks have to be large enough ($\sim 10^5 - 10^6 M_{\odot}$) to make stars (e.g. Tegmark et al. 1997; Abel et al. 1998; Fuller & Couchman 2000; Yoshida et al. 2003), one massive Population III star is enough to blow out the gas (e.g. Bromm et al. 2003). Also, note that the explosion does not have

to enrich the IGM of the entire universe, only needs to enrich the nearby IGM which re-infalls to the system. If this is the case, the oldest stars in the dSph has the signature, i.e. abundance pattern, of the first supernova explosion (e.g. Beasley et al. 2003). Hence, low metallicity stars in dSph may be the best target to look for the signature of the first stars (e.g. Sadakane et al. 2004).

Another problem in our simulated galaxy is too less luminous and too small velocity dispersion. We have tried the different parameter sets of models for star formation and SNe feedback. However, we found that to keep metallicity as low as what is observed, the strong SNe feedback that leads to the low efficiency of star formation is required, which makes it difficult to produce enough stars at a high redshift. The most simple solution is that tens of such small systems merge together without any additional star formation. However, it is unlikely, and such mergers make a metallicity gradient shallower (White 1980). Another solution would be that they were more massive. The virial mass of our galaxy is $5 \times 10^7 M_{\odot}$ at $z \sim 6$. The dynamical analysis of the dSphs suggests that their mass to light ratio is more than hundred (e.g. Kleyna et al. 2001; Hayashi et al. 2003), which suggests that the total mass of the Scl dSph is more than $10^8 M_{\odot}$. If the system is big enough, they might be able to continue a low level of star formation even after the re-ionization in the inner region along the scenario 3) described above. If this is the case, it would help to solve “the missing satellite problem” (Klypin et al. 1999; Moore et al. 1999) as discussed in Hayashi et al. (2003). Unfortunately, we have so far carried out the simulations from only one initial condition. For further investigation, it would be required to run simulations with different initial conditions with different patterns of small scale density perturbations, which lead to different mass systems with different merger histories.

Our simulation demonstrates that the recently available detailed properties of the observed dSph provide invaluable information about their formation history. Our current cosmological simulations obviously miss, or oversimplify, some important physics. For example, our SNe feedback model is too simple, and/or the resolution of our simulation is not good enough to describe SNe feedback, although the present study shows that the effect of SNe would be crucial to explain the observed properties of the dSph. Also, the IMF might depend on the physical condition of the progenitor gas, such as metallicity. In

addition, our simulation ignores the radiative transfer effects, such as radiative heating and pressure. The strong light from new born stars would suppress cooling of the surrounding gas, which would be important in the small system (Ricotti et al. 2002; Kitayama & Yoshida 2005). Nevertheless, the dSph is a good laboratory for studying the physical process of the galaxy formation. We hope that our present study would be a good starting point to test the formation scenario of the dSph, comparing the detailed observation with chemo-dynamical galaxy formation models.

We thank Andrew McWilliam for his helpful advice during the completion of this manuscript. This work is

partly supported by NSF AST-0206299, AST-0407176, NASA NAG5-13381, and a Grant-in-Aid for Scientific Research (No.16540223) by the Japanese Ministry of Education, Culture, Sports, Science and Technology. The financial support of the JSPS, through Postdoctoral Fellowship for research abroad, and the Australian Research Council, through its Discovery Project scheme, is gratefully acknowledged. We acknowledge the Astronomical Data Analysis Center of the National Astronomical Observatory, Japan (project ID: wna15b), the Institute of Space and Astronautical Science of Japan Aerospace Exploration Agency, and the Australian and Victorian Partnerships for Advanced Computing, where the numerical computations for this paper were performed.

APPENDIX

A. UPDATED VERSION OF GCD+

This study focuses on a small system which is forming at a high redshift, with a high resolution cosmological simulation. To follow the physics in such small scale, we have updated our original galactic chemodynamical evolution code, **GCD+**. In addition, we have changed some parameter values in the code from previous our studies (e.g. Kawata & Gibson 2003a,b). Below we explain what have been updated.

A.1. Radiative cooling with non-equilibrium chemical reaction of hydrogen and helium species

In the updated version, the code follows non-equilibrium chemical reaction of hydrogen and helium species (H , H^+ , He , He^+ , He^{++} , H_2 , H_2^+ , H^-), and their cooling processes. We assume the ionization equilibrium cooling for radiative cooling of heavy elements, because it is too expensive to follow the non-equilibrium chemical reaction of all the ionization states of the elements heavier than helium. Thus, the total cooling rate is the summation of equilibrium cooling of heavy elements and non-equilibrium cooling of hydrogen and helium. The equilibrium cooling of heavy elements is calculated using a code based on Raymond-Smith code (Raymond & Smith 1977) which is used in Cen et al. (1995).

We follow the non-equilibrium chemical reaction of species related to hydrogen and helium, i.e. H , H^+ , He , He^+ , He^{++} , H_2 , H_2^+ , H^- and e^- , and calculate their radiative cooling rate, based on the method of Abel et al. (1997); Anninos et al. (1997). Although Abel et al. (1997) used hydrogen molecular cooling rate of Lepp & Shull (1983), we adopt an updated one suggested by Galli & Palla (1998). The time-scales of radiative cooling and chemical reaction of these species are much smaller than the dynamical time-scale (Anninos et al. 1997; Yoshida et al. 2003). Therefore, we use sub-timesteps to calculate the chemical reaction and integrate the thermal equation. The code considers that the time-scale of chemical reaction is represented by the time-scale of change in number of free electron, $\tau_{sp} = n_e/\dot{n}_e$. The time-scale for radiative cooling is calculated by $\tau_{rad} = e/|\Lambda - \Gamma|$, where e is thermal energy, and Λ and Γ are the cooling and heating⁷ rate, respectively. For each gas particle, i , we set the sub-timestep to be $\Delta t_{sub,i} = \tau_{dyn}/2^n \leq \min(\epsilon\tau_{sp}, \epsilon\tau_{rad})$ with $\epsilon = 0.1$, for efficient integration. Here, τ_{dyn} is minimum timestep required from dynamical evolution, Δt_{dyn} (Kawata 1999). Following Anninos et al. (1997), we update the number, $n_{k,i}$, of k -th species in a gas particle, i , by a backward differentiation method, $n_{k,i}^{t+\Delta t_{sub,i}} = (C_{k,i}^{t+\Delta t_{sub,i}} \Delta t_{sub,i} + n_{k,i}^t)/(1 + D_{k,i}^{t+\Delta t_{sub,i}} \Delta t_{sub,i})$. Here, $C_{k,i}$ and $D_{k,i}$ are creation and destruction rate, respectively. The thermal energy is updated by semi-implicit method in our code. Note that Anninos et al. (1997) use the explicit method. However, we found that the semi-implicit method is more robust (K. Yoshikawa private communication). We solve the following equation with iteration.

$$u_i^{t+\Delta t_{sub,i}} = u_i^t + \Delta t_{sub,i} \frac{\Delta E_{SN,i}(t_n, \Delta t_{dyn})}{\Delta t_{dyn}} + 0.5 \Delta t_{sub,i} \left[\left(\frac{du}{dt} \right)_{ad,i}^{t_n} + \left(\frac{du}{dt} \right)_{ad,i}^{t_n + \Delta t_{dyn}} + \frac{\Gamma_i^t - \Lambda_i^t}{\rho_{g,i}} + \frac{\Gamma_i^{t+\Delta t_{sub,i}} - \Lambda_i^{t+\Delta t_{sub,i}}}{\rho_{g,i}} \right]. \quad (A1)$$

Here, $\Delta E_{SN,i}(t_n, \Delta t_{dyn})$ is the heating energy from SNe within the dynamical time step from t_n which indicates the time at the beginning of this sub-timestep integration. Also, $(du/dt)_{ad,i}$ is adiabatic term (Kawata 1999) for thermal equation. Since $(du/dt)_{ad,i}$ requires neighbor particle search which is computationally expensive, we use a mean value of $(du/dt)_{ad,i}$ at $t = t_n$ and $t = t_n + \Delta t_{dyn}$. Thus, the code re-calculates only radiative cooling and heating term at the sub-timestep, $t + \Delta t_{sub,i}$, i.e. $\Gamma_i^{t+\Delta t_{sub,i}}$ and $\Lambda_i^{t+\Delta t_{sub,i}}$, and the other terms are fixed. In addition, for simplicity, we assume that the gas density does not change dramatically within Δt_{dyn} , i.e. the gas density is assumed to be constant with $\rho_{g,i}^{t_n + \Delta t_{dyn}}$, during these sub-timesteps.

A.2. Yields

It is well known that the iron yield suggested in Woosley & Weaver (1995) seems to be overestimated, and leads to much lower $[\alpha/Fe]$, compared to $[\alpha/Fe]$ observed in low-metallicity stars in solar neighborhood. Since iron yield is the

⁷ In this paper, we do not take into account any background radiation. Thus, there is no photo-ionization heating.

most ambiguous yield for SNe II nucleosynthesis model, it is discussed that the half of their suggested yield is more appropriate (e.g. Timmes et al. 1995). Therefore, the updated code adopts the half of the yield of iron in Woosley & Weaver (1995).

A.3. Star formation criteria

The criteria of star formation are also changed from what were adopted in Kawata & Gibson (2003a). In the updated code, the Jeans unstable condition and density threshold are excluded from the criteria. Instead, we introduced a new criterion that the cooling time has to be smaller than dynamical time, i.e. $t_{\text{cool}} = e/|\Lambda - \Gamma| < t_{\text{dyn}} = \sqrt{3\pi/16G\rho}$ and $\Lambda > \Gamma$. Finally, this cooling time criterion and the convergence of the gas velocity field, $\nabla \cdot \mathbf{v}_i < 0$, are the criteria for star formation in the updated code. The Jeans unstable condition is discarded, because it is sensitive to the numerical resolution (Okamoto et al. 2003). The density threshold is ignored, because it is not well understood whether or not there is such threshold, except for disk galaxies. Additionally, for disk galaxies it is explained by the dynamical instability condition of the rotating gas disk (Kennicutt 1989), which should be able to be naturally taken into account in dynamical simulations.

REFERENCES

Abel, T., Anninos, P., Norman, M. L., & Zhang, Y. 1998, ApJ, 508, 518
 Abel, T., Anninos, P., Zhang, Y., & Norman, M. L. 1997, New Astronomy, 2, 181
 Anninos, P., Zhang, Y., Abel, T., & Norman, M. L. 1997, New Astronomy, 2, 209
 Arimoto, N., & Yoshii, Y. 1987, A&A, 173, 23
 Arnone, E., Ryan, S. G., Argast, D., Norris, J. E., & Beers, T. C. 2005, A&A, 430, 507
 Baade, W. 1944, ApJ, 100, 137
 Beasley, M. A., Kawata, D., Pearce, F. R., Forbes, D. A., & Gibson, B. K. 2003, ApJ, 596, L187
 Benson, A. J., Frenk, C. S., Lacey, C. G., Baugh, C. M., & Cole, S. 2002, MNRAS, 333, 177
 Bertschinger, E. 2001, ApJS, 137, 1
 Bressan, A., Chiosi, C., & Fagotto, F. 1994, ApJS, 94, 63
 Bromm, V., Yoshida, N., & Hernquist, L. 2003, ApJ, 596, L135
 Bullock, J. S., Kravtsov, A. V., & Weinberg, D. H. 2000, ApJ, 539, 517
 Carlberg, R. G. 1984, ApJ, 286, 403
 Carraro, G., Chiosi, C., Girardi, L., & Lia, C. 2001, MNRAS, 327, 69
 Cen, R., Kang, H., Ostriker, J. P., & Ryu, D. 1995, ApJ, 451, 436
 Chiba, M., & Nath, B. B. 1994, ApJ, 436, 618
 Dekel, A., & Silk, J. 1986, ApJ, 303, 39
 Efstathiou, G. 1992, MNRAS, 256, 43P
 Fuller, T. M., & Couchman, H. M. P. 2000, ApJ, 544, 6
 Gallagher, J. S., & Wyse, R. F. G. 1994, PASP, 106, 1225
 Galli, D., & Palla, F. 1998, A&A, 335, 403
 Geisler, D., Smith, V. V., Wallerstein, G., Gonzalez, G., & Charbonnel, C. 2005, AJ, 129, 1428
 Gibson, B. K. 1997, MNRAS, 290, 471
 Grebel, E. K. 1997, Reviews of Modern Astronomy, 10, 29
 Gregg, L. 1997, MNRAS, 285, 151
 Gregg, L., & Renzini, A. 1983, A&A, 118, 217
 Hayashi, E., Navarro, J. F., Taylor, J. E., Stadel, J., & Quinn, T. 2003, ApJ, 584, 541
 Ikuta, C., & Arimoto, N. 2002, A&A, 391, 55
 Kawata, D. 1999, PASJ, 51, 931
 Kawata, D., & Gibson, B. K. 2003a, MNRAS, 340, 908
 —. 2003b, MNRAS, 346, 135
 Kennicutt, R. C. 1989, ApJ, 344, 685
 Kitayama, T., & Suto, Y. 1996, ApJ, 469, 480
 Kitayama, T., & Yoshida, N. 2005, ApJ, in press,
 Kleyne, J. T., Wilkinson, M. I., Evans, N. W., & Gilmore, G. 2001, ApJ, 563, L115
 Klypin, A., Kravtsov, A. V., Valenzuela, O., & Prada, F. 1999, ApJ, 522, 82
 Kobayashi, C. 2004, MNRAS, 347, 740
 Kobayashi, C., & Arimoto, N. 1999, ApJ, 527, 573
 Kobayashi, C., Tsujimoto, T., & Nomoto, K. 2000, ApJ, 539, 26
 Kodama, T., & Arimoto, N. 1997, A&A, 320, 41
 Kunkel, W. E., & Demers, S. 1977, ApJ, 214, 21
 Larson, R. B. 1974, MNRAS, 166, 585
 Lepp, S., & Shull, J. M. 1983, ApJ, 270, 578
 Mateo, M. L. 1998, ARA&A, 36, 435
 McWilliam, A., & Smecker-Hane, T. A. 2005a, in ASP Conf. Ser. 336: Cosmic Abundances as Records of Stellar Evolution and Nucleosynthesis, 221–+
 McWilliam, A., & Smecker-Hane, T. A. 2005b, ApJ, 622, L29
 Mo, H. J., & White, S. D. M. 1996, MNRAS, 282, 347
 Moore, B., Ghigna, S., Governato, F., Lake, G., Quinn, T., Stadel, J., & Tozzi, P. 1999, ApJ, 524, L19
 Mori, M., Ferrara, A., & Madau, P. 2002, ApJ, 571, 40
 Okamoto, T., Jenkins, A., Eke, V. R., Quilis, V., & Frenk, C. S. 2003, MNRAS, 345, 429
 Raiteri, C. M., Villata, M., & Navarro, J. F. 1996, A&A, 315, 105
 Raymond, J. C., & Smith, B. W. 1977, ApJS, 35, 419
 Ricotti, M., & Gnedin, N. Y. 2002, ApJ, in press,
 Ricotti, M., Gnedin, N. Y., & Shull, J. M. 2002, ApJ, 575, 49
 Sadakane, K., Arimoto, N., Ikuta, C., Aoki, W., Jablonka, P., & Tajitsu, A. 2004, PASJ, 56, 1041
 Shetrone, M., Venn, K. A., Tolstoy, E., Primas, F., Hill, V., & Kaufer, A. 2003, AJ, 125, 684
 Smecker-Hane, T. A., & McWilliam, A. 2002, astro-ph, 0205411
 Spergel, D. N., Verde, L., Peiris, H. V., Komatsu, E., Nolta, M. R., Bennett, C. L., Halpern, M., Hinshaw, G., Jarosik, N., Kogut, A., Limon, M., Meyer, S. S., Page, L., Tucker, G. S., Weiland, J. L., Wollack, E., & Wright, E. L. 2003, ApJS, 148, 175
 Susa, H., & Umemura, M. 2004a, ApJ, 600, 1
 —. 2004b, ApJ, 610, L5
 Tegmark, M., Silk, J., Rees, M. J., Blanchard, A., Abel, T., & Palla, F. 1997, ApJ, 474, 1
 Thoul, A. A., & Weinberg, D. H. 1996, ApJ, 465, 608
 Timmes, F. X., Woosley, S. E., & Weaver, T. A. 1995, ApJS, 98, 617
 Tinsley, B. M. 1975, ApJ, 197, 159
 Tolstoy, E. 2005, astro-ph, 0506481
 Tolstoy, E., Irwin, M. J., Helmi, A., Battaglia, G., Jablonka, P., Hill, V., Venn, K. A., Shetrone, M. D., Letarte, B., Cole, A. A., Primas, F., Francois, P., Arimoto, N., Sadakane, K., Kaufer, A., Szeifert, T., & Abel, T. 2004, ApJ, 617, L119
 Tolstoy, E., Venn, K. A., Shetrone, M., Primas, F., Hill, V., Kaufer, A., & Szeifert, T. 2003, AJ, 125, 707
 van den Bergh, S. 1962, AJ, 67, 486
 van den Hoek, L. B., & Groenewegen, M. A. T. 1997, A&AS, 123, 305
 White, S. D. M. 1980, MNRAS, 191, 1P
 White, S. D. M., & Rees, M. J. 1978, MNRAS, 183, 341
 Woosley, S. E., & Weaver, T. A. 1995, ApJS, 101, 181
 Yoshida, N., Abel, T., Hernquist, L., & Sugiyama, N. 2003, ApJ, 592, 645